# In Silico Discovery of Multistep Chemistry Initiated by a Conical Intersection: The Challenging Case of Donor Acceptor Stenhouse Adducts

David M. Sanchez,[1,2,#] Umberto Raucci,[1,2,&] and Todd J. Martínez[1,2]

[1]*Stanford PULSE Institute, SLAC National Accelerator Laboratory, Menlo Park, USA.*
[2]*Department of Chemistry, Stanford University, Stanford, USA.*

## Abstract

Detailed mechanistic understanding of multistep chemical reactions triggered by internal conversion via a conical intersection is a challenging task that emphasizes limitations in theoretical and experimental techniques. Hypothesis-driven methodologies (e.g. characterization of critical points and biased molecular dynamics) are commonly employed to explore chemical space and simulate reaction events. In this contribution, we present a discovery-based, hypothesis-free computational approach based on first principles molecular dynamics to discover and refine the switching mechanism of Donor-Acceptor Stenhouse Adducts (DASAs). Using state-of-the-art graphical processing units-enabled electronic structure calculations we performed in total ~2ns of adiabatic and non-adiabatic *ab initio* molecular dynamics discovering a) critical intermediates that are involved in the open-to-closed transformation, b) several competing pathways which lower the overall switching yield, and c) key elements for future design strategies. Our dynamics describe the natural evolution of both the nuclear and electronic degrees of freedom that govern the interconversion between DASA ground state intermediates exposing significant elements for the future design strategies of molecular switches.

[#]*Present address: Design Physics Division, Lawrence Livermore National Laboratory, Livermore, USA.*
[&]*Present address: Italian Institute of Technology, Genova GE, Italy*

Photomechanical materials are an emerging frontier in the design and fabrication of photoactuators due to their extraordinary ability to convert light energy into macroscopic work.[1-7] The molecular engine behind these complex architectures is represented by molecular photoswitches capable of reversible interconversion between two isomers upon light irradiation.[8] Despite significant progress in improving and designing molecular photoswitches, the race to find the "*holy grail"* is far from complete: small fatigue resistance, photo/thermal instabilities, limited light penetration, and suboptimal excited-state features represent the Achilles' heel of many common families of purposed molecular photoswitches[9-14] (e.g. spiropyrans, diarylethene, and azobenzenes in Figure 1a). In addition to these shortcomings, their rather simple 1-step photoswitching mechanism involving a single reaction coordinate (e.g. photoisomerization, electrocyclization) and picosecond (or faster) time scales inherently hinders the design and development of novel candidates that are based on similar photoreactive moieties. As a result, the next generation of molecular photoswitches could benefit greatly from a more complex multistep mechanism consisting of tunable intermediates that can be exploited to target a range of desired functionality (Figure 1b).

Donor-Acceptor Stenhouse Adducts[15-19] (DASAs) are a novel class of photoswitches that incorporate complexity by introducing tunable structural features in the form of donor and acceptor groups linked together via a hydroxylated triene bridge that can be systematically altered to influence their multistep photoswitching behavior (Figure 1b**).** These switches display a rich and complex multistep mechanism consisting of photoisomerization, 4π-electrocyclization, and proton transfer (PT) processes[20-26] (Figure 1b), which, unlike previous single reaction coordinate molecular photoswitches, improves their ability to be tailored to a range of practical applications (e.g. smart materials,[27-31] photopharmacology,[9,32-36] nano

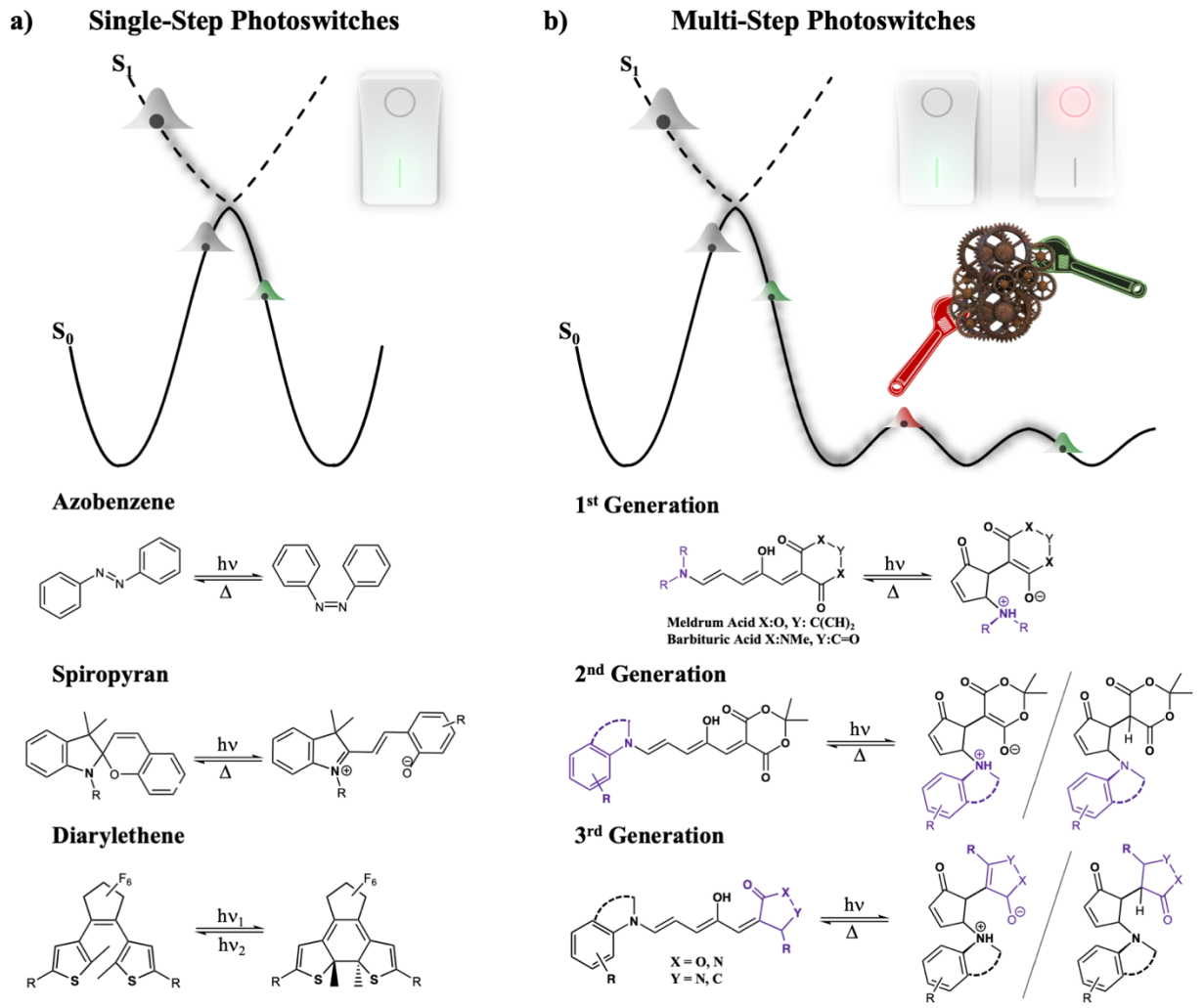


**Figure 1. a)** Previous photomechanical switches (azobenzene, spiropyran, and diarylethene) undergo a simple, 1-step mechanism consisting of photoisomerization and bond breaking, respectively. **b)** DASAs are tunable photomechanical switches that consist of a donor and acceptor group that undergo an array of multistep chemical reactions on the ground state upon relaxation through a conical interaction. The different DASA generations are shown in purple.

systems,[37-39] and receptors[40-42]). Exploiting the properties of these promising molecules to design purposed photosensitive materials ultimately hinges upon the ability to understand and control their stepwise dynamics at the molecular level. Several experimental and theoretical studies have been performed to unravel the DASA switching mechanism, but key intermediates and their interconnecting pathways have yet to be fully characterized. For example, rapid scan infrared (IR) and transient absorption spectroscopy identified the open/closed forms (reactant and

products) of the complete reaction[20-26] (Figure 1b), but these techniques are quite limited when identifying short-lived intermediates with similar structure and electronic properties. Additionally, traditional hypothesis-driven computational approaches have been employed[43-45] to propose possible reaction pathways, but this strategy rests on the assumption that photoinduced processes follow equilibrium dynamics and that the optimization of a single reaction pathway is sufficient to describe the inherent dynamical behavior of DASA's chemistry.

In this contribution we present a discovery-based, hypothesis-free computational approach based on first principles molecular dynamics to discover and refine the complex switching mechanism of Meldrum's acid 1st generation DASA. *Ab initio* Multiple Spawning (AIMS)[46-49] coupled to TeraChem[50-52] was used to describe the initial photoisomerization and generate a set of initial conditions to explore the ground state PES via Born-Oppenheimer molecular dynamics (BOMD) (computational details are provided in the Supplementary Information). Using non-adiabatic and adiabatic *ab initio* quantum molecular dynamics, we identified critical intermediates that are involved in the open-to-closed transformation and several competing pathways, which shed light on key elements for future design strategies.

The DASA switching mechanism is initiated by the absorption of 545nm light, promoting the open-form (**A**, Figure 2), initially in the EEZZ configuration (E/Z labels refer to the E/Z configuration assumed by the ω, δ, α, β bonds, respectively), to an electronically excited state via a ππ* transition (molecular orbitals involved in the transition are shown in Figure S1). In our recent theoretical study,[53] we showed that **A** primarily relaxes back to the ground state forming **A'** (EEEZ) through a **Z**/**E** photoisomerization consisting of a one-bond flip around the $C_3$-$C_4$ double bond (α in Figure 2). During the internal conversion through the conical intersection, all of the incident photon's energy is transferred into nuclear kinetic energy which at short

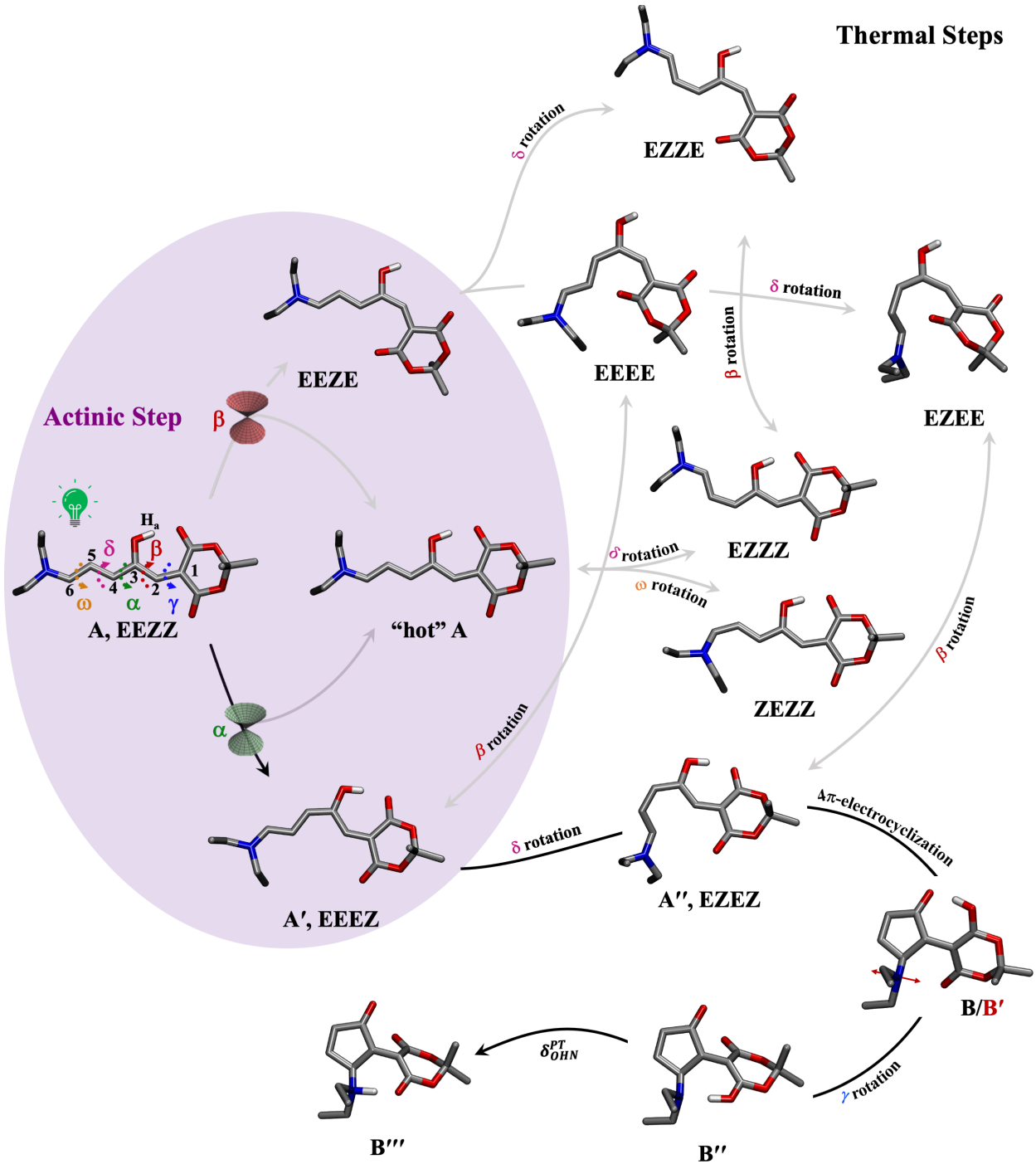


**Figure 2.** The full 4π-electrocyclization pathway (black) along with all alternate pathways (grey) discovered during the ab initio dynamics. Labels for dihedral angles and carbon atoms are shown along the hexatriene bridge. Each "open" structure is labeled according to the E/Z configuration assumed by the ω, δ, α, β bonds, respectively. All protons are emitted for clarity except for $H_a$. Movies from the discovery-based dynamics and the Cartesian coordinates of the $S_0$ minima shown above are provided in the SI-Files.

timescales (before internal vibrational energy redistribution) is concentrated in a few vibrational modes along the backbone of **A'**. As a consequence, the molecule explores several configurations and reaction pathways that could be inaccessible in an equilibrium regime. In addition to the productive pathway along α, Figure 2 shows several competing channels are possible upon nonradiative decay to the ground-state due to isomerization around alternate dihedral angles of the hexatriene bridge. In the following, we quantify our findings by following the wavepacket dynamics during the course of the discovery-based ground-state dynamics.

In Figure 3, we show how the energy absorbed via the incident photon manifests in nuclear motion highlighting the time-evolution of the crucial intermediates along the discovered pathways in Figure 2. Isomers are histogrammed based on their dihedral angles (α, β, γ, δ, and ω), $C_2$-$C_6$ and N-$H_a$ distances (see Figure S2 for details on the binning criteria). Ten ps after electronic excitation, we observe a photoisomerization branching ratio between **A** and **A'** of 55:15 (Figure 3a), which is in agreement with the measured DASA photoisomerization yield of approximately 21% of **A'** in toluene.[21] After 500fs, the EEEZ intermediate (**A'**) begins to form reaching a maximum of 20% around 2.2ps (Figure 3a). Then, the population in **A'** slowly begins to decrease due to the further rotation around $C_4$-$C_5$ bond the (δ in Figure 2) and the subsequent formation of approximately 17% of the EZEZ intermediate, **A".** The dynamics show that the excess rotational momentum gained by the donor group from the α isomerization promotes a subsequent rotation around δ (i.e. the formation of **A"**). At ~6.5 and 9 ps, the population of **A'** and **A"** invert as further rotation of δ drives **A"** back to **A'** and vice versa. The formation of **A"** leads to a shortening of the $C_2$-$C_6$ distance (Figure S3) promoting the carbon-carbon bond formation and a trace amount (less than 1%) of the closed cyclopentenone form, **B**. The shortening of the $C_2$-$C_6$ distance is highly coupled to the PT from the hydroxyl

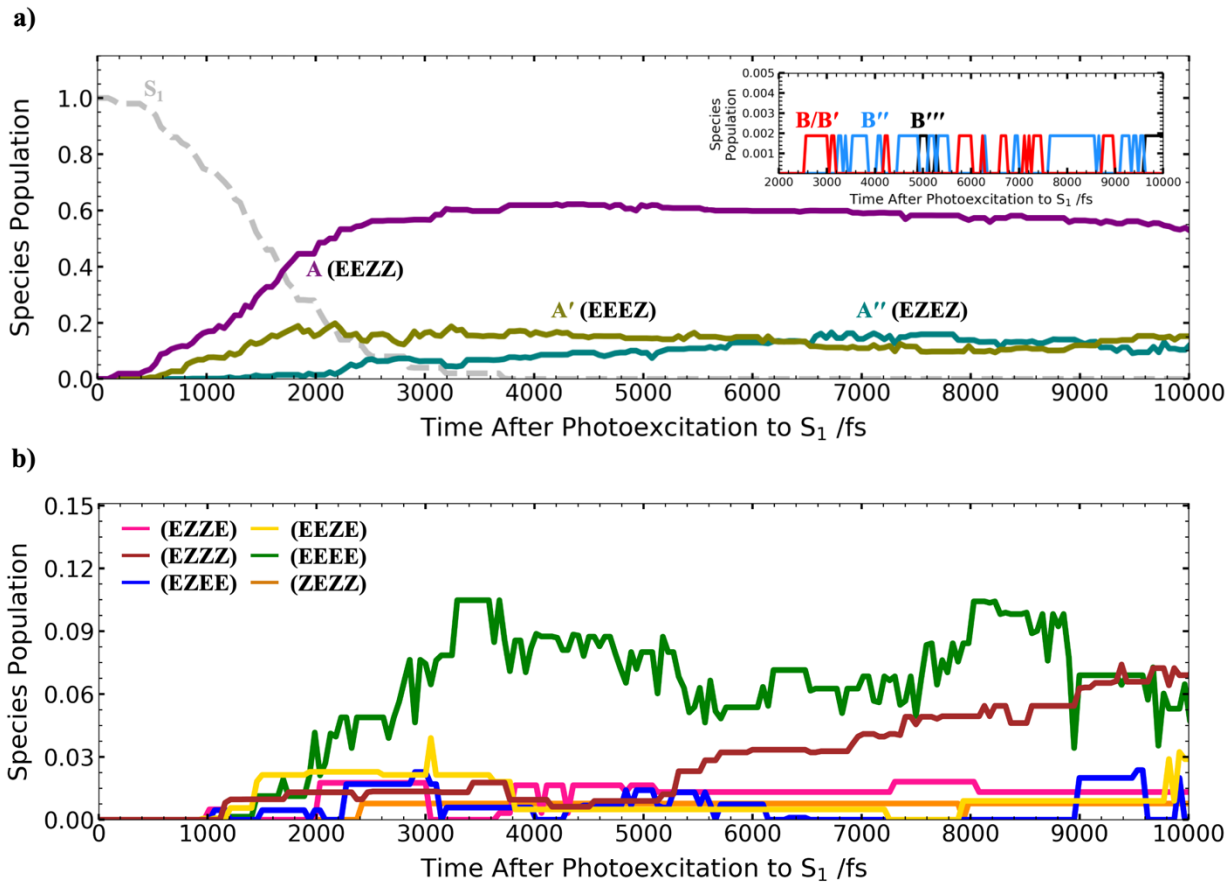


**Figure 3. a)** The population of DASA species at time *t* of the first 10ps of the AIMS/BOMD trajectories. Only contributions to intermediates undergoing 4π-electrocyclization are shown for clarity. The formation of **B/B′**, **B″**, and **B‴** are followed in the inset. A movie for the full productive pathway is available in SI-Files (A-B‴-Full-Pathway.mov). **b)** The population of all discovered alternate DASA species. The binning criteria are shown in Figure S2. All populations represent an incoherent sum over all 236 trajectory basis functions with 186 of these on the ground state every 50fs.

group to the neighboring carbonyl oxygen. This suggests that one may be able to promote the ring-closing reaction by strengthening the intramolecular hydrogen bond (i.e. increasing the basicity of the acceptor group). In the inset of Figure 3a, we show the rise of population at 2.5 ps corresponding to the formation of **B**/**B'** and the subsequent interconversion between **B"** and **B"'**, which we investigate further in the following.

Continuing along the productive pathway leading to the zwitterionic form, **B"** is formed after the rotation around the $C_1$-$C_2$ bond (γ in Figure 2) which brings the hydroxyl group close to

the donor moiety. The pyramidalization of the donor nitrogen atom is an important degree of freedom involved in the dynamics of the **B**-type species. Indeed, the nitrogen atom freely inverts for all **A** and **B** intermediates due to excess energy via dynamics through a CI. Large fluctuations (± 60°) are observed in **B** (Figure S4), making it difficult to distinguish **B** conformers based on the nitrogen pyramidalization alone. This refines the mechanism hypothesized by Zulfikri et al.[25] where a **B'** intermediate (characterized by inversion about N) has been proposed. Once **B"** is formed, the PT between the hydroxyl group and the nitrogen atom leads to ~1% of the final zwitterionic form (**B'"**). The nitrogen pyramidalization and the PT coordinate are tightly coupled in this step: the orientation of the nitrogen towards the hydroxyl group promotes PT and leads to the formation of the zwitterionic form (Figure S5). Influencing the nitrogen pyramidalization through steric effects might be an effective avenue to change the final yield of the zwitterionic form.

Lastly, we show a rich and diverse ground-state chemistry triggered by interconversion through the $S_0/S_1$ CI. The ground-state consists of a complex interplay of interlinking reactions involving rotations about different carbon-carbon bonds along the hexatriene bridge. These alternate pathways make up a nontrivial (~20%) portion of the total wavepacket on the ground state, making their tunability important to improve DASA photoswitching yield and efficiency. Figure 3b shows the time-evolution of the population for all alternate pathways discovered during the course of the ground-state dynamics. Upon the formation of **A'**, the wavepacket bifurcates evenly between an EEEE intermediate and **A"** (both ~10%) due to the symmetric nature of the internal vibrational redistribution around α to β (EEEE) or δ (**A"**). Not only would strengthening the intramolecular hydrogen bond promote the previously mentioned **A"** to **B** transformation, but it may also inhibit rotation around β and the subsequent formation of the

EEEE intermediate. At approximately 1.5ps, we observe the formation of an EZEE intermediate that arises due to rotation of δ in the EEEE intermediate. An alternate pathway to form EZEE was observed via A", where rotation around δ was followed by isomerization around the $C_2$-$C_3$ bond (β in Figure 2). Our previous simulations revealed 22% of the wavepacket followed an alternate nonradiative relaxation pathway involving the isomerization around β, resulting in approximately 4% EEZE intermediate. At 2ps, we observe the formation of a relatively long-lived EZZE intermediate resulting from rotation around the $C_5$-$C_6$ bond (ω in Figure 2). Additionally, we showed the majority of the wavepacket (~64%) returns back to the photoreactant forming "hot" EEZZ. Being sufficiently "hot," approximately 7% of the wavepacket continues on to isomerize around δ forming an EZZZ intermediate that has been observed by Feringa and coworkers.[25] On a later timescale, we observe the formation of a ZEZZ intermediate as a result of rotation around ω, which also has been hypothesized via static calculations but, until now, has yet to be confirmed.

In conclusion, we have shown for the first time the complete photoswitching mechanism for Meldrum's Acid 1st generation DASAs using a discovery-based computational approach based on *ab initio* molecular dynamics. Our AIMS/BOMD simulation showed the natural evolution of the wavepacket across multiple ground-state species upon relaxing through the CI on the picosecond timescale. Additionally, we showed the key structural parameters involved in each step of DASA's multistep photoswitching mechanism, providing new insights to better control the photoswitching mechanism. Overall, our ground- and excited-state dynamics suggest that the intramolecular hydrogen bond represents a key design parameter for inducing not only the **Z**/**E** photoisomerization in the actinic step, but also the 4π-electrocyclization on the ground-state. Also, we show a rich and diverse ground-state chemistry involving a complex interplay of

interlinking reactions involving rotations about different carbon-carbon bonds along the hexatriene bridge on timescales that can compete with the productive photoswitching pathway. This study provides unprecedent details of the complete photoswitching mechanism of DASAs and showcases the state-of-the-art tools in unraveling complex, multistep, photoinitiated ground-state chemistry.

**Acknowledgments**

This work was supported by the MURI program of the Office of Naval Research (N00014-18-1-2624 and N00014-18-1-2659). Lawrence Livermore National Laboratory is operated by Lawrence Livermore National Security, LLC, for the U.S. Department of Energy, National Nuclear Security Administration under Contract DE-AC52-07NA27344.

**Supporting Information**

Computational details for AIMS and BOMD, the AIMS Method Review, extracting population from AIMS for observed species, SA-CASSCF natural orbitals, binning criteria for ground-state intermediates, evolution of $\alpha$, $\beta$, $\gamma$, and $C_2$-$C_6$ carbon-carbon bond evolution for the complete photoinitiated 4$\pi$-electrocyclization pathway (**A**-**B'''**) for the coordinate expectation value of a representative trajectory, and movies for the interconversion between all steps in Figure 2. Additionally, Cartesian coordinates are included for optimized structures of all species reported in Figure 2.

## References


(1) Browne, W. R.; Feringa, B. L. Chiroptical molecular switches. *Mol. Switches* **2011**, *1*, 121.
(2) Hugel, T.; Holland, N. B.; Cattani, A.; Moroder, L.; Seitz, M.; Gaub, H. E. Single-molecule optomechanical cycle. *Science* **2002**, *296*, 1103.
(3) Irie, M.; Kobatake, S.; Horichi, M. Reversible surface morphology changes of a photochromic diarylethene single crystal by photoirradiation. *Science* **2001**, *291*, 1769.
(4) Kim, T.; Zhu, L.; Al-Kaysi, R. O.; Bardeen, C. J. Organic photomechanical materials. *ChemPhysChem* **2014**, *15*, 400.
(5) Tanchak, O. M.; Barrett, C. J. Light-induced reversible volume changes in thin films of azo polymers: the photomechanical effect. *Macromolecules* **2005**, *38*, 10566.
(6) White, T. J. *Photomechanical Materials, Composites, and Systems: Wireless Transduction of Light into Work*; Wiley, 2017.
(7) Yu, Y.; Nakano, M.; Ikeda, T. Photomechanics: directed bending of a polymer film by light. *Nature* **2003**, *425*, 145.
(8) Wegner, H. A. Molecular Switches. Second Edition. Edited by Ben L. Feringa and Wesley R. Browne. *Ang. Chem. Int. Ed.* **2012**, *51*, 2281.
(9) Beharry, A. A.; Woolley, G. A. Azobenzene photoswitches for biomolecules. *Chem. Soc. Rev.* **2011**, *40*, 4422.
(10) Bleger, D.; Hecht, S. Visible-light-activated molecular switches. *Ang. Chem. Int. Ed.* **2015**, *54*, 11338.
(11) Irie, M.; Fukaminato, T.; Matsuda, K.; Kobatake, S. Photochromism of diarylethene molecules and crystals: memories, switches, and actuators. *Chem. Rev.* **2014**, *114*, 12174.
(12) Tian, H.; Yang, S. Recent progresses on diarylethene based photochromic switches. *Chem. Soc. Rev.* **2004**, *33*, 85.
(13) Perrier, A.; Maurel, F.; Jacquemin, D. Single Molecule Multiphotochromism with Diarylethenes. *Acc. Chem. Res.* **2012**, *45*, 1173.
(14) Yang, C.; Slavov, C.; Wegner, H. A.; Wachtveitl, J.; Dreuw, A. Computational design of a molecular triple photoswitch for wavelength-selective control. *Chem. Sci.* **2018**, *9*, 8665.
(15) Helmy, S.; Oh, S.; Leibfarth, F. A.; Hawker, C. J.; Read de Alaniz, J. Design and Synthesis of Donor–Acceptor Stenhouse Adducts: A Visible Light Photoswitch Derived from Furfural. *J. Org. Chem.* **2014**, *79*, 11316.
(16) Helmy, S.; Leibfarth, F. A.; Oh, S.; Poelma, J. E.; Hawker, C. J.; Read de Alaniz, J. Photoswitching Using Visible Light: A New Class of Organic Photochromic Molecules. *J. Amer. Chem. Soc.* **2014**, *136*, 8169.
(17) Hemmer, J. R.; Page, Z. A.; Clark, K. D.; Stricker, F.; Dolinski, N. D.; Hawker, C. J.; Read de Alaniz, J. Controlling Dark Equilibria and Enhancing Donor–Acceptor Stenhouse Adduct Photoswitching Properties through Carbon Acid Design. *J. Amer. Chem. Soc.* **2018**, *140*, 10425.
(18) Hemmer, J. R.; Poelma, S. O.; Treat, N.; Page, Z. A.; Dolinski, N. D.; Diaz, Y. J.; Tomlinson, W.; Clark, K. D.; Hooper, J. P.; Hawker, C.; Read de Alaniz, J. Tunable Visible and Near Infrared Photoswitches. *J. Amer. Chem. Soc.* **2016**, *138*, 13960.
(19) Mallo, N.; Brown, P. T.; Iranmanesh, H.; MacDonald, T. S. C.; Teusner, M. J.; Harper, J. B.; Ball, G. E.; Beves, J. E. Photochromic switching behaviour of donor–acceptor Stenhouse adducts in organic solvents. *Chem. Comm.* **2016**, *52*, 13576.
(20) Di Donato, M.; Lerch, M. M.; Lapini, A.; Laurent, A. D.; Iagatti, A.; Bussotti, L.; Ihrig, S. P.; Medved', M.; Jacquemin, D.; Szymański, W.; Buma, W. J.; Foggi, P.; Feringa, B. L.

Shedding Light on the Photoisomerization Pathway of Donor–Acceptor Stenhouse Adducts. *J. Amer. Chem. Soc.* **2017**, *139*, 15596.
(21) Lerch, M. M.; Di Donato, M.; Laurent, A. D.; Medved', M.; Iagatti, A.; Bussotti, L.; Lapini, A.; Buma, W. J.; Foggi, P.; Szymański, W. Solvent Effects on the Actinic Step of Donor–Acceptor Stenhouse Adduct Photoswitching. *Ang. Chem. Int. Ed.* **2018**, *57*, 8063.
(22) Lerch, M. M.; Medved′, M.; Lapini, A.; Laurent, A. D.; Iagatti, A.; Bussotti, L.; Szymanski, W.; Buma, W. J.; Foggi, P.; Di Donato, M. Tailoring Photoisomerization Pathways in Donor–Acceptor Stenhouse Adducts: The Role of the Hydroxy Group. *J. Phys. Chem. A* **2018**, *122*, 955.
(23) Lerch, M. M.; Szymański, W.; Feringa, B. L. The (photo) chemistry of Stenhouse photoswitches: guiding principles and system design. *Chem. Soc. Rev.* **2018**, *47*, 1910.
(24) Lerch, M. M.; Wezenberg, S. J.; Szymanski, W.; Feringa, B. L. Unraveling the Photoswitching Mechanism in Donor–Acceptor Stenhouse Adducts. *J. Amer. Chem. Soc.* **2016**, *138*, 6344.
(25) Zulfikri, H.; Koenis, M. A. J.; Lerch, M. M.; Di Donato, M.; Szymański, W.; Filippi, C.; Feringa, B. L.; Buma, W. J. Taming the Complexity of Donor–Acceptor Stenhouse Adducts: Infrared Motion Pictures of the Complete Switching Pathway. *J. Amer. Chem. Soc.* **2019**, *141*, 7376.
(26) Bull, J. N.; Carrascosa, E.; Mallo, N.; Scholz, M. S.; da Silva, G.; Beves, J. E.; Bieske, E. J. Photoswitching an Isolated Donor–Acceptor Stenhouse Adduct. *J. Phys. Chem. Lett.* **2018**, *9*, 665.
(27) Wang, L.; Li, Q. Photochromism into nanosystems: towards lighting up the future nanoworld. *Chem. Soc. Rev.* **2018**, *47*, 1044.
(28) Heinke, L.; Cakici, M.; Dommaschk, M.; Grosjean, S.; Herges, R.; Bräse, S.; Wöll, C. Photoswitching in Two-Component Surface-Mounted Metal–Organic Frameworks: Optically Triggered Release from a Molecular Container. *ACS Nano* **2014**, *8*, 1463.
(29) Li, Q.; Fuks, G.; Moulin, E.; Maaloum, M.; Rawiso, M.; Kulic, I.; Foy, J. T.; Giuseppone, N. Macroscopic contraction of a gel induced by the integrated motion of light-driven molecular motors. *Nature Nanotech.* **2015**, *10*, 161.
(30) Ohshima, S.; Morimoto, M.; Irie, M. Light-driven bending of diarylethene mixed crystals. *Chem. Sci.* **2015**, *6*, 5746.
(31) Pianowski, Z. L.; Karcher, J.; Schneider, K. Photoresponsive self-healing supramolecular hydrogels for light-induced release of DNA and doxorubicin. *Chem. Comm.* **2016**, *52*, 3143.
(32) Velema, W. A.; Szymanski, W.; Feringa, B. L. Photopharmacology: Beyond Proof of Principle. *J. Amer. Chem. Soc.* **2014**, *136*, 2178.
(33) Frank, J. A.; Yushchenko, D. A.; Hodson, D. J.; Lipstein, N.; Nagpal, J.; Rutter, G. A.; Rhee, J.-S.; Gottschalk, A.; Brose, N.; Schultz, C.; Trauner, D. Photoswitchable diacylglycerols enable optical control of protein kinase C. *Nature Chem. Bio.* **2016**, *12*, 755.
(34) Babii, O.; Afonin, S.; Garmanchuk, L. V.; Nikulina, V. V.; Nikolaienko, T. V.; Storozhuk, O. V.; Shelest, D. V.; Dasyukevich, O. I.; Ostapchenko, L. I.; Iurchenko, V.; Zozulya, S.; Ulrich, A. S.; Komarov, I. V. Direct Photocontrol of Peptidomimetics: An Alternative to Oxygen-Dependent Photodynamic Cancer Therapy. *Ang. Chem. Int. Ed.* **2016**, *55*, 5493.
(35) Fujimoto, K.; Kajino, M.; Sakaguchi, I.; Inouye, M. Photoswitchable, DNA-Binding Helical Peptides Assembled with Two Independently Designed Sequences for Photoregulation and DNA Recognition. *Chem. Eur. J.* **2012**, *18*, 9834.
(36) Zhu, M.; Zhou, H. Azobenzene-based small molecular photoswitches for protein modulation. *Org. Biomol. Chem.* **2018**, *16*, 8434.

(37) Kim, D.; Jeong, K.; Kwon, J. E.; Park, H.; Lee, S.; Kim, S.; Park, S. Y. Dual-color fluorescent nanoparticles showing perfect color-specific photoswitching for bioimaging and super-resolution microscopy. *Nature Comm.* **2019**, *10*, 3089.
(38) Goulet-Hanssens, A.; Eisenreich, F.; Hecht, S. Enlightening Materials with Photoswitches. *Adv. Mat.* **2020**, *32*, 1905966.
(39) Bisoyi, H. K.; Li, Q. Light-Directing Chiral Liquid Crystal Nanostructures: From 1D to 3D. *Acc. Chem. Res.* **2014**, *47*, 3184.
(40) Gómez-Santacana, X.; de Munnik, S. M.; Mocking, T. A. M.; Hauwert, N. J.; Sun, S.; Vijayachandran, P.; de Esch, I. J. P.; Vischer, H. F.; Wijtmans, M.; Leurs, R. A toolbox of molecular photoswitches to modulate the CXCR3 chemokine receptor with light. *Beilstein J. Org. Chem.* **2019**, *15*, 2509.
(41) Izquierdo-Serra, M.; Bautista-Barrufet, A.; Trapero, A.; Garrido-Charles, A.; Díaz-Tahoces, A.; Camarero, N.; Pittolo, S.; Valbuena, S.; Pérez-Jiménez, A.; Gay, M.; García-Moll, A.; Rodríguez-Escrich, C.; Lerma, J.; de la Villa, P.; Fernández, E.; Pericàs, M. À.; Llebaria, A.; Gorostiza, P. Optical control of endogenous receptors and cellular excitability using targeted covalent photoswitches. *Nature Comm.* **2016**, *7*, 12221.
(42) Alfimov, M. V.; Fedorova, O. A.; Gromov, S. P. Photoswitchable molecular receptors. *J. Photochem. Photobio. A* **2003**, *158*, 183.
(43) García-Iriepa, C.; Marazzi, M. Level of theory and solvent effects on DASA absorption properties prediction: comparing TD-DFT, CASPT2 and NEVPT2. *Materials* **2017**, *10*, 1025.
(44) García-Iriepa, C.; Marazzi, M.; Sampedro, D. From Light Absorption to Cyclization: Structure and Solvent Effects in Donor-Acceptor Stenhouse Adducts. *ChemPhotoChem* **2019**, *0*.
(45) Laurent, A. D.; Medveď, M.; Jacquemin, D. Using Time-Dependent Density Functional Theory to Probe the Nature of Donor–Acceptor Stenhouse Adduct Photochromes. *ChemPhysChem* **2016**, *17*, 1846.
(46) Ben-Nun, M.; Martínez, T. J. Ab initio quantum molecular dynamics. *Adv. Chem. Phys.* **2002**, *121*, 439.
(47) Ben-Nun, M.; Martínez, T. J. Nonadiabatic molecular dynamics: Validation of the multiple spawning method for a multidimensional problem. *J. Chem. Phys.* **1998**, *108*, 7244.
(48) Ben-Nun, M.; Quenneville, J.; Martínez, T. J. Ab Initio Multiple Spawning: Photochemistry from First Principles Quantum Molecular Dynamics. *J. Phys. Chem. A* **2000**, *104*, 5161.
(49) Yang, S.; Martínez, T. J. *Ab initio multiple spawning: First principles dynamics around conical intersections*; World Scientific: Singapore, 2011; Vol. 17.
(50) Ufimtsev, I. S.; Martinez, T. J. Quantum Chemistry on Graphical Processing Units. 2. Direct Self-Consistent-Field Implementation. *J. Chem. Theory Comput.* **2009**, *5*, 1004.
(51) Ufimtsev, I. S.; Martinez, T. J. Quantum chemistry on graphical processing units. 3. Analytical energy gradients, geometry optimization, and first principles molecular dynamics. *J. Chem. Theory Comput.* **2009**, *5*, 2619.
(52) Ufimtsev, I. S.; Martínez, T. J. Quantum Chemistry on Graphical Processing Units. 1. Strategies for Two-Electron Integral Evaluation. *J. Chem. Theory Comput.* **2008**, *4*, 222.
(53) Sanchez, D. M.; Raucci, U.; Ferreras, K. N.; Martínez, T. J. Putting Photomechanical Switches to Work: An Ab Initio Multiple Spawning Study of Donor–Acceptor Stenhouse Adducts. *J. Phys. Chem. Lett.* **2020**, *11*, 7901.

# SUPPLEMENTAL INFORMATION: IN SILICO DISCOVERY OF MULTISTEP CHEMISTRY INITIATED BY A CONICAL INTERSECTION: THE CHALLENGING CASE OF DONOR ACCEPTOR STENHOUSE ADDUCTS

David M. Sanchez,[1,2,#] Umberto Raucci,[1,2,&] and Todd J. Martínez[1,2]

[1]*Stanford PULSE Institute, SLAC National Accelerator Laboratory, Menlo Park, USA.*
[2]*Department of Chemistry, Stanford University, Stanford, USA.*

Supplementary Information table of contents:



[#]*Present address: Design Physics Division, Lawrence Livermore National Laboratory, Livermore, USA.*
[&]*Present address: Italian Institute of Technology, Genova GE, Italy*

## I. Computational Details

The full photoinitiated ring-closing mechanism of Meldrum's acid 1st generation Donor-Acceptor Stenhouse Adducts (DASA) in the gas phase is investigated using *ab initio* multiple spawning[1-3] (AIMS) and Born-Oppenheimer molecular dynamics (BOMD). We simulate the first 10 ps of ultrafast dynamics for Meldrum acid 1st generation DASA by: 1) using AIMS to propagate the initial wavepacket for the first 5ps or until all population has returned to the ground state, 2) stopping TBFs on the ground state when they are decoupled from other TBFs (off-diagonal elements of the Hamiltonian become small), and 3) adiabatically continuing these stopped TBFs using the positions and momenta from the last frame in AIMS as initial conditions for discovery-based BOMD. This method has been shown to work well in describing photoinitiated ground-state chemistry.[4,5]

For the AIMS dynamics, we used GPU-accelerated State-Averaged Complete Active Space Self Consistent Field theory[6-8] (SA-CASSCF) consisting of an active space of two electrons in two orbitals determined to minimize the average energy of the lowest three singlet states, in conjunction with the 6-31G** basis set, i.e. SA3-CAS(2,2)SCF/6-31G**. The first three singlet states ($S_0$, $S_1$, and $S_2$) are included in the dynamics. The adaptive timestep was set to 0.48 fs (20 au) (reduced to 0.12 fs (5 au) in regions with large nonadiabatic coupling) and used to propagate the centers of the trajectory basis functions (TBFs). A coupling threshold of 0.01 au (scalar product of nonadiabatic coupling and velocity vectors) initiates spawning events generating new TBFs on different electronic states. Population transfer between TBFs is described by solving the time-dependent Schrödinger equation in the time-evolving TBF basis set. We refer the reader elsewhere for details regarding these AIMS simulations.[9]

For the discovery-based BOMD dynamics on the ground state, we employ unrestricted Density Functional Theory (DFT) with the Perdew-Burke-Ernzerhof hybrid exchange-correlation functional,[10] i.e uPBE0-D3/6-31G**. The BOMD was sampled according to the microcanonical ensemble (NVE) (i.e. fixed number of atoms, volume, and energy) using a fixed timestep of 0.5 fs. All electronic structure calculations (i.e. energies, gradients, and nonadiabatic coupling vectors (NACV)) are performed with the TeraChem electronic structure package.[11-13] A total of 236 TBFs are propagated during the course of the entire simulation, with 186 of these being adiabatically continued on the ground state with DFT. Cartesian coordinates of all $S_0$ intermediates discovered during the adiabatic dynamics were optimized at the uPBE0-D3/6-31G** level of theory and included in the SI-Files.

**II. *Ab Initio* Multiple Spawning**

*Ab initio* multiple spawning (AIMS) is a nonadiabatic dynamics algorithm aimed at describing photodynamical processes involving multiple electronic states using a time-dependent basis set. In the following, we present a brief introduction to the working equations of AIMS and refer the reader elsewhere for a more a more detailed discussion.[14] The exact molecular wavefunction can be separated into electronic and nuclear contributions using the Born-Huang representation:

$$\Psi\left(\mathbf{r},\mathbf{R},t\right)=\sum_{I}\chi_{I}\left(\mathbf{R},t\right)\phi_{I}\left(\mathbf{r};\mathbf{R}\right) \tag{1}$$

where $\chi_{I}\left(\mathbf{R},t\right)$ denotes the time-dependent nuclear wavefunction for electronic state I and $\phi_{I}\left(\mathbf{r};\mathbf{R}\right)$ is the electronic wavefunction for state I at nuclear configuration **R**. In the adiabatic representation, $\phi_{I}\left(\mathbf{r};\mathbf{R}\right)$ is expanded into an orthonormal electronic basis consisting of eigenfunctions of the time-independent electronic Schrödinger equation (TIESE) parametrically

dependent on nuclear configuration **R**. Under the AIMS ansatz, $\chi_I(\mathbf{R},t)$ is represented as a superposition of frozen Gaussian functions called trajectory basis functions (TBF):

$$\chi_I(\mathbf{R},t) = \sum_{k=1}^{N_I(t)} c_k^I(t)\chi_k^I\left(\mathbf{R};\bar{\mathbf{R}}_k^I(t),\bar{\mathbf{P}}_k^I(t),\bar{\gamma}_k^I(t),\alpha_k^I\right) \tag{2}$$

where $N_I(t)$ is the total number of TBFs on electronic state I, $c_k^I(t)$ is the time-dependent complex coefficient of the *k*th TBF on electronic state I, $\boldsymbol{\alpha}_k^I$ is the frozen TBF width, and $\chi_k^I(...)$ is a multidimensional frozen Gaussian that is expressed as a product of one-dimensional Gaussian functions corresponding to the 3N nuclear degrees of freedom. In AIMS, each TBF evolves adiabatically along one Born-Oppenheimer electronic surface. The time-dependent positions and momenta, $\left(\bar{R}_{\rho_k}^I(t),\bar{P}_{\rho_k}^I(t)\right)$, of the TBFs are propagated classically according to Hamilton's equations of motion on the given electronic state:

$$\frac{\partial \bar{\mathrm{R}}_{\rho_k}^I(t)}{\partial t} = \frac{\bar{\mathrm{P}}_{\rho_k}^I(t)}{m_\rho} \tag{3}$$

$$\frac{\partial \bar{P}_{\rho_k}^I(t)}{\partial t} = -\left.\frac{\partial E_I(\mathbf{R})}{\partial R_{\rho_k}}\right|_{\bar{R}_{\rho_k}^I(t)} \tag{4}$$

where $m_\rho$ is the mass for the $\rho$th nuclear coordinate and $E_I(\mathbf{R})$ is the electronic energy of state I with nuclear configuration **R**. The nuclear phase, $\bar{\gamma}_k^I(t)$, is propagated semiclassically according to the classical Lagrangian:

$$\frac{\partial \bar{\gamma}_k^I}{\partial t} = \sum_{\rho=1}^{3N} \frac{\left(\bar{P}_{\rho_k}^I(t)\right)^2}{2m_\rho} - E_I\left(\bar{\mathbf{R}}_k^I(t)\right) \tag{5}$$

The evolution of the time-dependent amplitudes is governed by the time-dependent Schrodinger equation (TDSE) written in matrix form as:

$$\frac{d\mathbf{C}^{I}(t)}{dt} = -i\left(\mathbf{S}_{II}^{-1}\right)\left\{\left[\mathbf{H}_{II} - i\dot{\mathbf{S}}_{II}\right]\mathbf{C}^{I} + \sum_{J\neq I}\mathbf{H}_{IJ}\mathbf{C}^{J}\right\} \tag{6}$$

where **S** and $\dot{\mathbf{S}}$ are the nuclear overlap matrix and its right-acting time-derivative, respectively, and **H** is the Hamiltonian. The matrix elements of the Hamiltonian are computed using the zeroth-order saddle-point (SP) approximation, which involves evaluating the zeroth-order Taylor expansion of the PES and/or nonadiabatic coupling vector (NACV) around the centroid position between pairs of TBFs. In addition to the SP approximation, the independent first generation (IFG) approximation is used to describe the initial nuclear wavepacket at time t = 0 as a swarm of independent initial TBFs each with their own positions and momenta sampled from a harmonic Wigner distribution, i.e. initial conditions (IC). Unlike the initial TBFs, the spawned TBFs from each IC remain coupled during the course of the dynamics and their separation naturally accounts for decoherence of the nuclear wavefunction on multiple electronic states.

## III. Classifying Isomers from Structural Dynamics on $S_0$

The natural evolution of the wavepacket dynamics can be followed by binning geometries along ground-state TBFs into one of the DASA photoproducts (**A, A', A'', B/B', B'', B''', EEZE, EZEE, EZZE, EEEE, EZZZ, and ZEZZ),** following previous studies.[5] Snapshots taken every 50fs along all 186-ground state DFT TBFs were binned into one of the isomers based on dihedral angles (α, β, γ, δ, ω) and atomic distances ($C_2$-$C_6$ and N-$H_a$). For details on the binning criteria, see Supplementary **Fig. S1**. Due to the ground state TBFs being sufficiently uncoupled from all others, the population for a given isomer at time *t* of TBF *k* of IC *M* can be computed as:

$$n_k^M(t) = \left| c_k^M(t) \right|^2 \tag{7}$$

where the total population of a specific isomer *L* at time t on the ground-state, $P_L(t)$ is computed by:

$$P_L(t) = \frac{1}{N_{IC}} \sum_{M=1}^{N_{IC}} \left[ \frac{\sum_k^{N_{TBF}^M(t)} c_{k,M}^*(t)\, c_{k,M}(t)\, \delta\left(L, I\left(\bar{R}_{k,M}(t)\right)\right)}{\sum_k^{N_{TBF}^M(t)} c_{k,M}^*(t)\, c_{k,M}(t)} \right] \tag{8}$$

where *L* is defined as one of **(A**, **A'**, **A"**, **B/B'**, **B"**, **B"'**, **EEZE**, **EZEE**, **EZZE**, **EEEE**, **EZZZ**, and **ZEZZ**), $c_{k,M}(t)$ is the amplitude of the *k*th TBF and *M*th IC, $N_{IC}$ is the total number of initial conditions, and $\delta(\ldots)$ is a Kronecker-delta function, and $I(R)$ represents the isomer classification of the geometry given by *R*.

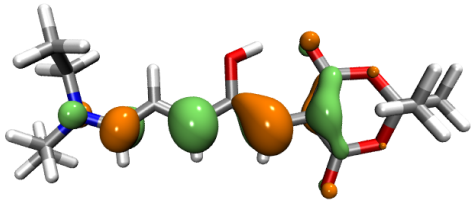

**Orbital 80**

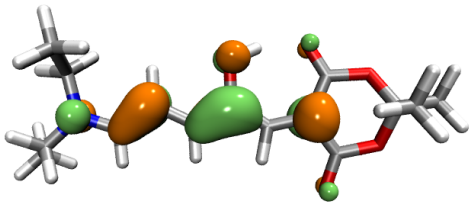

**Orbital 79**

**Figure S1.** The SA3-CAS(2,2)SCF/6-31G** natural orbitals at the $S_0$ minimum. Orange and green correspond to 0.05 and-0.05e-/Å$^3$ isovalues, respectively.

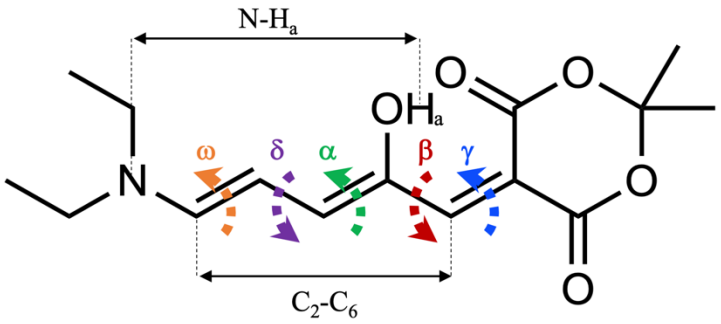


| Isomer | Binning Criteria | | | | | | |
|---|---|---|---|---|---|---|---|
| | α (°) | β (°) | γ (°) | δ (°) | ω (°) | $C_2$-$C_6$ (Å) | N-$H_a$ (Å) |
| **A** | ≥ 100 | ≥ 100 | ≥ 100 | ≥ 100 | ≥ 100 | ≥ 2.0 | ≥ 2.0 |
| **A'** | **≤ 80** | ≥ 100 | ≥ 100 | ≥ 100 | ≥ 100 | ≥ 2.0 | ≥ 2.0 |
| **A"** | **≤ 80** | ≥ 100 | ≥ 100 | **≤ 80** | ≥ 100 | ≥ 2.0 | ≥ 2.0 |
| **B/B'** | **≤ 80** | ≥ 100 | ≥ 100 | **≤ 80** | ≥ 100 | **< 2.0** | ≥ 2.0 |
| **B"** | **≤ 80** | ≥ 100 | **≤ 80** | **≤ 80** | ≥ 100 | **< 2.0** | ≥ 2.0 |
| **B'"** | **≤ 80** | ≥ 100 | **≤ 80** | **≤ 80** | ≥ 100 | **< 2.0** | **< 2.0** |
| **EEZE** | ≥ 100 | **≤ 80** | ≥ 100 | ≥ 100 | ≥ 100 | ≥ 2.0 | ≥ 2.0 |
| **EEEE** | **≤ 80** | **≤ 80** | ≥ 100 | ≥ 100 | ≥ 100 | ≥ 2.0 | ≥ 2.0 |
| **EZZZ** | ≥ 100 | ≥ 100 | ≥ 100 | **≤ 80** | ≥ 100 | ≥ 2.0 | ≥ 2.0 |
| **ZEZZ** | ≥ 100 | ≥ 100 | ≥ 100 | ≥ 100 | **≤ 80** | ≥ 2.0 | ≥ 2.0 |
| **EZZE** | **≤ 80** | **≤ 80** | ≥ 100 | ≥ 100 | ≥ 100 | ≥ 2.0 | ≥ 2.0 |
| **EZEE** | **≤ 80** | **≤ 80** | ≥ 100 | **≤ 80** | ≥ 100 | ≥ 2.0 | ≥ 2.0 |

**Figure S2.** Dihedral angle and atomic distance labels for structural parameters in DASA. Binning criteria used to classify isomers discovered during the ground-state adiabatic dynamics.

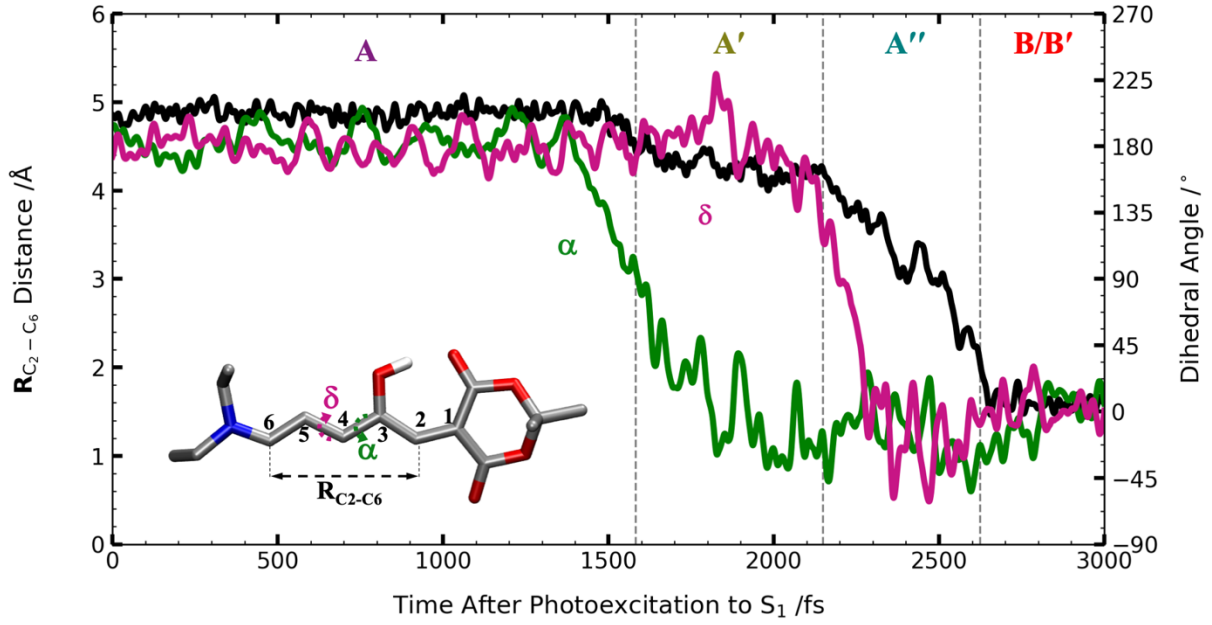


**Figure S3.** The complete 4π-electrocyclization pathway (characterized by the time evolution of α, δ, and the $C_2$-$C_6$ distance) for a representative trajectory of the AIMS/BOMD simulation. A three-step mechanism can be clearly identified: 1) isomerization around α forms **A'** 2) subsequent rotation of δ forms **A"** 3) shortening of $C_2$-$C_6$ distance leads to **B**. In the first 1.6ps, the molecule exists in the **A** configuration, where both α and δ are approximately 180° and the $C_2$-$C_6$ distance oscillates around 4.8Å. Upon relaxation through the $S_1/S_0$ CI at ~1.6ps, α begins to twist 90° resulting in a shortening of the $C_2$-$C_6$ distance by 0.5Å and the formation of **A'**. At approximately 2.2ps, the δ angle begins to twist leading to the formation of **A"**. Once **A"** is formed at ~2.6ps, the $C_2$-$C_6$ distance shortens to ~1.55Å, providing an optimal arrangement for the carbon-carbon bond formation leading to the closed cyclopentanone form **B**.

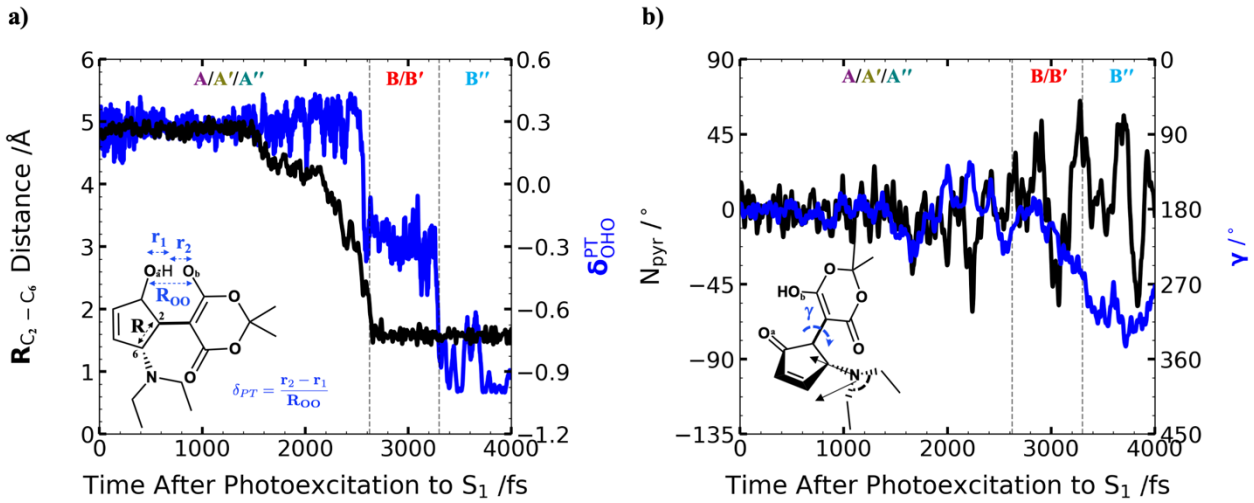


**Figure S4.** In **a**, the time evolution of the $C_2$-$C_6$ distance and proton transfer (PT) coordinate between the hydroxyl and neighboring carbonyl oxygens ($\delta_{OHO}^{PT}$) shows a highly coupled motion, resulting in a clear distinction between **A/A'/A"** and **B**-type intermediates. In the first 2.5 ps, $\delta_{OHO}^{PT}$ oscillates around 0.3 (with small fluctuations of the hydrogen bond), and a stable $O_aH$ bond is observed in the **A/A'/A"** species. The formation of **A"** leads to a significant decrease of the $C_2$-$C_6$ distance, which is accompanied by the PT from the hydroxyl to the carbonyl group at 2.6 ps (i.e. $\delta_{OHO}^{PT}$ changes sign). Next, the decrease in $\delta_{OHO}^{PT}$ marks the formation of **B** when the hydrogen bound to $O_a$ transfers to $O_b$. Around 3.3 ps, a second jump in $\delta_{OHO}^{PT}$ is observed from -0.3 to -0.9 when the $O_a$-$O_b$ hydrogen bond is disrupted due to rotation in γ, leading to the formation of **B"**. In **b**, we show the time evolution of $N_{pyr}$ and its coupling with the γ rotation which reveals that the nitrogen freely inverts for all **A** and **B** intermediates due to excess energy via dynamics through a CI. Large fluctuations of the $N_{pyr}$ angle (± 60°) are observed in **B**, making it difficult to distinguish B conformers based on $N_{pyr}$ alone. This refines the mechanism hypothesized by Zulfikri et al. where a **B'** intermediate (characterized by inversion about N) has been proposed.[15]

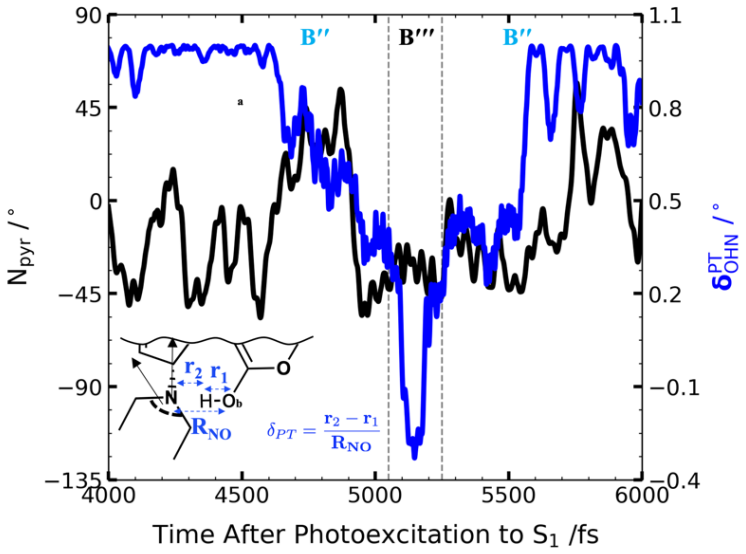


**Figure S5.** The coupling between $N_{pyr}$ and the PT coordinate between $O_b$ and the nitrogen $\left(\delta_{OHN}^{PT}\right)$ is evident in in the above figure. When the nitrogen is pyramidalized away from acceptor (positive $N_{pyr}$) poor interaction with the hydrogen inhibits the PT reaction ($\delta_{OHN}^{PT}$ oscillates around 0.5). At ~4.6 ps after the photoexcitation, the nitrogen inverts (negative $N_{pyr}$) and $\delta_{OHN}^{PT}$ decreases to 0.35. This orientation strengthens the hydrogen bond between the nitrogen and the hydrogen of $O_b$ via more favorable orbital overlap of the nitrogen lone pair and hydrogen, leading to the subsequent formation of **B'''**. However, the back-proton transfer from the nitrogen to $O_b$ is also observed after 5.25 ps, leading to a fast interconversion between **B''** and **B'''**.

**Movie Descriptions: DASA Excited- and Ground-State Chemistry Movies**

**(Movie: A-B'''-Full-Pathway.mov)** This movie was generated from the coordinate expectation value of a single AIMS trajectory basis function propagating first on $S_1$ and then spawned on $S_0$ using SA3-CAS(2,2)-SCF/6-31G** and uPBE0/6-31G**, respectively. It shows the full DASA 1st generation photoswitching mechanism in isolation discovered using free NVE dynamics with no enhanced sampling techniques. DASA starts in the open linear from, **A**, at equilibrium on the ground-state. Upon excitation with light, DASA is promoted to an electronically excited-state, where it undergoes nonradiative relaxation via α or β nonradiative relaxations channels. On the ground-state, several pathways are accessible due to the absorbed energy of the photon. After forming **A**, a second isomerization takes place around δ resulting in the formation of **A''**. DASA then undergoes a concerted proton transfer and C-C bond formation, forming **B**. Lastly, DASA eventually twists around γ to form **B''**, which correctly orients the proton with the donor group nitrogen. The movie end with the transfer of the proton to the nitrogen forming the zwitterionic DASA intermediate, **B'''**. All subsequent steps shown in **Figure 2** were generated in the same way and are labeled accordingly (i.e. reactant-product.mov).

## References


(1) Ben-Nun, M.; Martínez, T. J. Nonadiabatic molecular dynamics: Validation of the multiple spawning method for a multidimensional problem. *J. Chem. Phys.* **1998**, *108*, 7244.
(2) Ben-Nun, M.; Quenneville, J.; Martínez, T. J. Ab Initio Multiple Spawning: Photochemistry from First Principles Quantum Molecular Dynamics. *J. Phys. Chem. A* **2000**, *104*, 5161.
(3) Ben-Nun, M.; Martínez, T. J. Ab initio quantum molecular dynamics. *Adv. Chem. Phys.* **2002**, *121*, 439.
(4) Mignolet, B.; Curchod, B. F.; Martínez, T. J. Rich Athermal Ground-State Chemistry Triggered by Dynamics through a Conical Intersection. *Angewandte Chemie (International ed. in English)* **2016**, *55*, 14993.
(5) Wolf, T. J. A.; Sanchez, D. M.; Yang, J.; Parrish, R. M.; Nunes, J. P. F.; Centurion, M.; Coffee, R.; Cryan, J. P.; Gühr, M.; Hegazy, K.; Kirrander, A.; Li, R. K.; Ruddock, J.; Shen, X.; Vecchione, T.; Weathersby, S. P.; Weber, P. M.; Wilkin, K.; Yong, H.; Zheng, Q.; Wang, X. J.; Minitti, M. P.; Martínez, T. J. The photochemical ring-opening of 1,3-cyclohexadiene imaged by ultrafast electron diffraction. *Nature Chem.* **2019**, *11*, 504.
(6) Snyder, J. W., Jr.; Fales, B. S.; Hohenstein, E. G.; Levine, B. G.; Martinez, T. J. A direct-compatible formulation of the coupled perturbed complete active space self-consistent field equations on graphical processing units. *J Chem Phys* **2017**, *146*, 174113.
(7) Snyder, J. W.; Curchod, B. F. E.; Martínez, T. J. GPU-Accelerated State-Averaged Complete Active Space Self-Consistent Field Interfaced with Ab Initio Multiple Spawning Unravels the Photodynamics of Provitamin D3. *J. Phys. Chem. Lett.* **2016**, *7*, 2444.
(8) Hohenstein, E. G.; Luehr, N.; Ufimtsev, I. S.; Martinez, T. J. An atomic orbital-based formulation of the complete active space self-consistent field method on graphical processing units. *J Chem Phys* **2015**, *142*, 224103.
(9) Sanchez, D. M.; Raucci, U.; Ferreras, K. N.; Martínez, T. J. Putting Photomechanical Switches to Work: An Ab Initio Multiple Spawning Study of Donor–Acceptor Stenhouse Adducts. *J. Phys. Chem. Lett.* **2020**, *11*, 7901.
(10) Adamo, C.; Barone, V. Toward reliable density functional methods without adjustable parameters: The PBE0 model. *J. Chem. Phys.* **1999**, *110*, 6158.
(11) Ufimtsev, I. S.; Martinez, T. J. Quantum Chemistry on Graphical Processing Units. 2. Direct Self-Consistent-Field Implementation. *J. Chem. Theory Comput.* **2009**, *5*, 1004.
(12) Ufimtsev, I. S.; Martinez, T. J. Quantum chemistry on graphical processing units. 3. Analytical energy gradients, geometry optimization, and first principles molecular dynamics. *J. Chem. Theory Comput.* **2009**, *5*, 2619.
(13) Ufimtsev, I. S.; Martínez, T. J. Quantum Chemistry on Graphical Processing Units. 1. Strategies for Two-Electron Integral Evaluation. *J. Chem. Theory Comput.* **2008**, *4*, 222.
(14) Curchod, B. F. E.; Martínez, T. J. Ab Initio Nonadiabatic Quantum Molecular Dynamics. *Chem. Rev.* **2018**, *118*, 3305.
(15) Zulfikri, H.; Koenis, M. A. J.; Lerch, M. M.; Di Donato, M.; Szymański, W.; Filippi, C.; Feringa, B. L.; Buma, W. J. Taming the Complexity of Donor–Acceptor Stenhouse Adducts: Infrared Motion Pictures of the Complete Switching Pathway. *J. Amer. Chem. Soc.* **2019**, *141*, 7376.